CFD MODELLING AND VALIDATION OF WALL CONDENSATION IN THE PRESENCE OF NON-CONDENSABLE GASES

G. Zschaeck[*], T. Frank[*] and A. D. Burns[▲]

[*]*ANSYS Germany GmbH, Staudenfeldweg 12, Otterfing, 83624, Germany*
[▲]*ANSYS UK Ltd, 97 Milton Park, Abingdon, Oxfordshire OX14 4RY, UK*

guillermo.zschaeck@ansys.com

Abstract: The aim of this paper is to present and validate a mathematical model implemented in ANSYS CFD for the simulation of wall condensation in the presence of non-condensable substances. The model employs a mass sink at isothermal walls or conjugate heat transfer (CHT) domain interfaces where condensation takes place. The model was validated using the data reported by Ambrosini et al. (2008) and Kuhn et al. (1997).

1. INTRODUCTION

During a postulated loss of coolant accident (LOCA) large amount of steam is released into the nuclear containment. Condensation on the containment walls is foreseen as one of several passive mechanisms to keep pressure below the design threshold in generation III and III+ reactors (de la Rosa, 2009).

In such scenario it is expected that the wall condensation process is hindered by the presence of non-condensable gases (e.g. air entrained in nuclear containment), since they accumulate at the liquid-gas interface creating a diffusion barrier for the water vapour.

In order to model the wall condensation in the presence of non-condensable gases by means of industrial CFD codes, several boundary condition formulations have been proposed in the past for laminar (e.g. Karkoszka and Anglart, 2008) and turbulent flows (e.g. Ambrosini, 2005; Houkema et al., 2008; Kelm, 2010). This paper describes the mathematical formulation of the wall condensation model for turbulent flows implemented in ANSYS CFX and its validation against two different laboratory scale cases.

2. MATHEMATICAL MODEL

The present model employs a mass sink at walls and CHT boundaries to a multi-component gaseous fluid, which is a mixture of condensable and non-condensable components. The mass sink simulates the removal of condensable components at walls which are sufficiently cold to permit condensation onto a thin liquid film at the wall.

The following main assumptions apply to the proposed wall condensation model (see also Figure 1):

- The fluid consists of a multi-component gaseous mixture with one condensable and at least one non-condensable component
- The condensation rate is driven by the concentration boundary layer
- The vapour is in thermal equilibrium with the liquid film at the interface, i.e. partial pressure is equal to its saturation pressure at the interface temperature
- The details of the liquid film are not modelled (single phase) and the mass of gaseous phase which is lost by condensation is removed from the system
- Wall functions are not influenced by wall suction
- At a CHT boundary, the latent heat released by condensation is assumed to be absorbed by the solid material at the interface

In a turbulent boundary layer, the mass fluxes M_{A_w} and M_{B_w} of a non-condensable component (A) and a condensable component (B) of a binary gaseous mixture are given by:

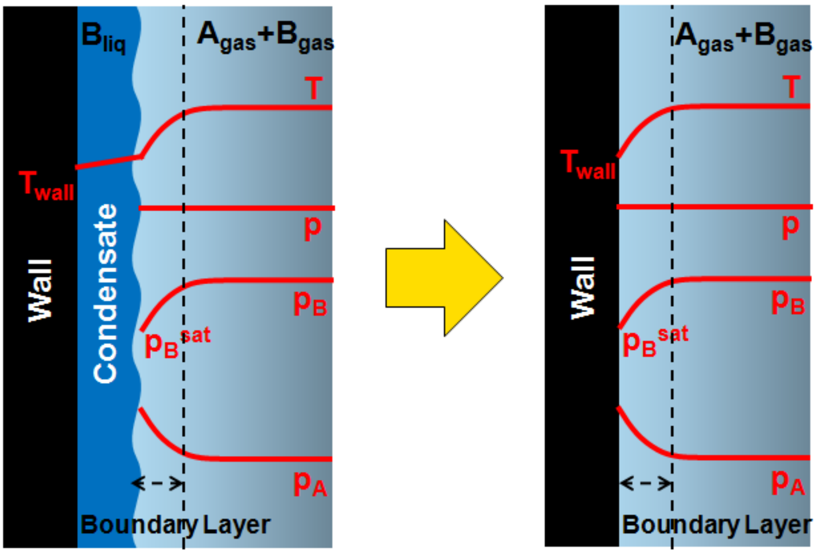

Figure 1. Wall condensation of component B in the presence of non-condensable gas A: left condensation process, right simplified model (adapted from Kelm, 2010)

$$M_{A_w} = M_{Mix} \cdot Y_{A_w} - k \cdot \rho \cdot \left(Y_{A_p} - Y_{A_w}\right) \tag{1}$$

$$M_{B_w} = M_{Mix} \cdot Y_{B_w} - k \cdot \rho \cdot \left(Y_{B_p} - Y_{B_w}\right) \tag{2}$$

where Y is the mass fraction, ρ the density and k is the turbulent mass transfer coefficient, which is a function of y^+ and the molecular Schmidt number as in Kader (1981). Here, w subscripts refer to wall quantities; p subscripts refer to near wall mesh points. The equations above are a special form of Fick's first law (Bird et al., 1960).

Since component A does not condensate, $M_{B_w} = M_{Mix}$. Hence, substituting into equation (2) and rearranging gives:

$$M_{B_w} = -k\left(y^+, Sc\right) \cdot \rho \cdot \frac{Y_{B_p} - Y_{B_w}}{1 - Y_{B_w}} \tag{3}$$

The value of Y_{B_p} is obtained from the solution of a transport equation for the condensable substance. The value of Y_{B_w} is calculated from the condensable component's molar fraction X_{B_w}, which is determined by assuming that the vapour is in thermal equilibrium with the liquid film at the interface, and hence its partial pressure is equal to its saturation pressure at the interface temperature. In reality, the vapour at the edge of the boundary layer may be a supersaturated wet vapour, or mist. Only the dry part of the vapour will form the concentration gradient which drives the condensation mass flux. Hence, only the molar fraction of dry vapour is used to determine the mass flux.

For the energy equation, two boundary conditions are allowed for the condensation model: isothermal wall and fluid-solid interface. In case of an isothermal wall boundary, the wall is assumed to constitute an infinite reservoir on which the effect of the condensation heat source is negligible; hence it is maintained at its constant temperature.

In case of a fluid-solid boundary, the latent heat released by condensation to the liquid film is assumed to be absorbed by the solid phase at the interface. This gives a heat source to the solid side:

$$Q = -M_{B_w} \cdot L \tag{4}$$

where L is the latent heat of vaporization. In contrast to previous implementations (e.g. Houkema et al., 2008; Kelm, 2010), the underlying algorithm for the mapping of the heat source term at the interface is fully parallelized for the unstructured coupled solver and allows the use of numerical grids with non-coincident nodes at the fluid-solid interface. The heat source was carefully linearized in order to enhance the numerical robustness of the model.

3. CONAN TEST CASE (Ambrosini et al., 2008)

3.1. EXPERIMENTAL FACILITY

The first validation case corresponds to the CONAN experimental facility as described by Ambrosini et al. (2005, 2008). It consists of a vertical square duct (primary test channel) in which a mixture of air and water vapour flows downwards while being cooled at one of the walls made of a 4.5 cm thick aluminium plate. The rear side of the plate is cooled by liquid water flowing upwards in a rectangular duct (secondary coolant channel) as depicted in Figure 2.

Ambrosini et al. (2008) measured the surface heat flux profile along the plate centreline as well as the condensate flow for several operating points.

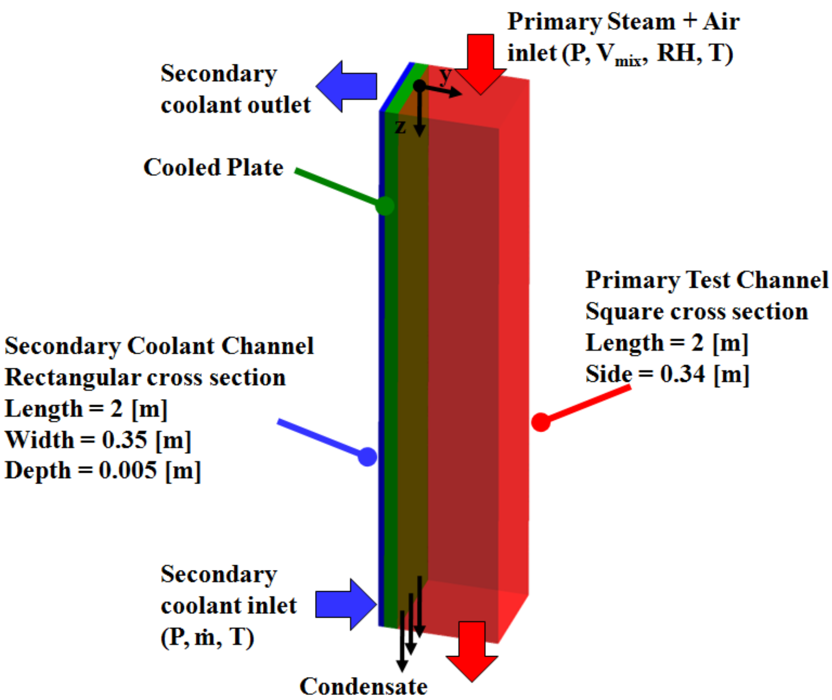

Figure 2. Sketch of the CONAN experimental facility (adapted from Ambrosini et al., 2008)

3.2. GEOMETRY AND MESHING

The original three-dimensional geometry shown in Figure 2 was simplified to a two-dimensional geometry as suggested by Ambrosini et al. (2008). This geometry was meshed with a quasi-two-dimensional hexahedral grid consisting of two fluid domains, namely cooling water and air-water vapour mixture, and one solid domain (aluminium plate).

Four different hexahedral grids were generated using ANSYS ICEM CFD 14.0. The properties of these grids are summarized in Table 1.

Table 1. Numerical grids properties

	Mesh 1	**Mesh 2**	**Mesh 3**	**Mesh 4**
Number of Nodes	13,630	45,824	220,448	783,894
Number of Elements	6,404	22,145	108,660	388,363
Max. Aspect Ratio	101.7	217.3	533.6	517.6
Avg. y^+ Prim. Sys.	20.3	4.82	0.98	0.52
Avg. y^+ Sec. Sys.	19.8	4.95	0.99	0.51

3.3. CFD-SETUP AND BOUNDARY CONDITIONS

The steady-state simulations for the CONAN test case were performed with ANSYS CFX 14.0, using the coupled double precision solver. The SST turbulence model of Menter (1994) was used for all calculations in conjunction with the automatic near wall treatment for ω-based models. The wall condensation model was activated at the domain interface between the aluminium plate and the primary test channel.

The fluid in the primary test channel was considered as an ideal multi-component mixture of air and water vapour, where air was treated as the constraint fluid material. The ideal gas equation of state was used for the air and the IAPWS-IF97 equation of state for the water vapour; the density of the cooling water was taken as constant. The molecular diffusivity of water vapour in air was taken from Poling et al. (2001).

A schematic representation of the applied boundary conditions is depicted in Figure 3.

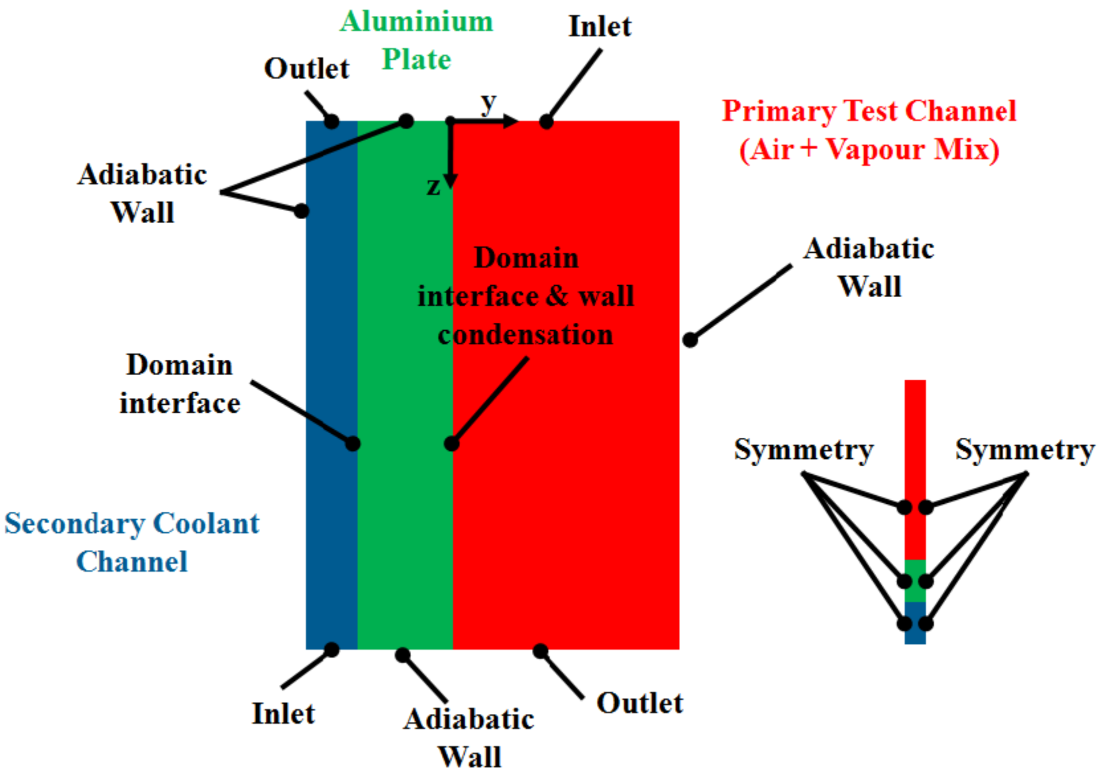

Figure 3. Boundary conditions for the CONAN test case

The inlet boundary conditions for the primary test channel and the secondary coolant channel are summarized in Table 2 for different experiments. Since turbulent quantities were not specified by the authors, these values were assumed ($Tu = 5\%$ and $\mu_t / \mu = 10$). An averaged static pressure boundary condition was applied at both outlets and set equal to 1 atm.

In order to achieve the steady-state convergence, a pseudo time-step of 5[ms] was used of the primary test channel domain, 100[ms] for the aluminium plate and 50[ms] for the secondary coolant channel. An under-relaxation factor of 0.3 was used for the condensation mass flux at the interface. For all transport equations the second order upwind scheme (High Resolution) was applied with the exception of the turbulence model equations. For these equations a first order upwind scheme was used.

Table 2. Inlet boundary conditions for the CONAN test case (Ambrosini et al., 2008)

Experiment	Primary Test Channel (Air-Water Vapour Mixture)			Secondary Coolant Channel (Liquid Water)	
	$V_{in, Mix}$ [m/s]	Rel. $Hum_{in,Mix}$ [%]	$T_{in, Mix}$ [°C]	$T_{in, H2O}$ [°C]	$\dot{m}_{in, H2O}$ [kg/s]
P10-T30-V15	1.46	100.0	82.66	31.24	1.217080
P10-T30-V20	2.02	100.0	80.61	31.10	1.217269
P10-T30-V25	2.52	97.83	79.13	31.07	1.216775
P10-T30-V30	3.01	87.35	78.73	30.91	1.216021
P10-T30-V35	3.59	96.55	75.02	30.71	1.215949

3.4. RESULTS

Before comparing the numerical results with the experimental data, the iteration and spatial discretisation errors were investigated using the best practice guidelines for CFD proposed by Menter (2002). In both cases, the target values were the condensation rate and the surface heat flux at the interface between the primary test channel and the aluminium plate. The aim of this investigation is to quantify and control the numerical errors in order to evaluate the predictive power of the wall condensation model.

For the iteration error investigation, the convergence criterion (maximum residual) was varied to measure its effects on the target values. From Figure 4 it can be stated that, for the condensation rate, a maximum residual of $1x10^{-4}$ is enough to keep the iteration error below 0.06%, therefore this criterion was used in subsequent calculations.

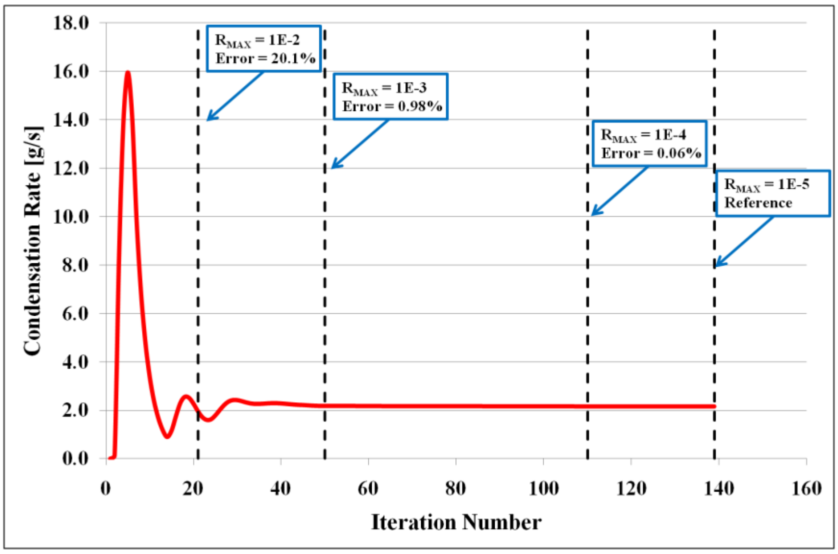

Figure 4. Condensation rate as a function of the iteration number (exp. P10-T30-V25, Mesh 3)

The simulations were carried out in four different grids in order to study the spatial discretisation error. The effect of the mesh refinement on the condensation rate is shown in Figure 5 (left), where the solution on meshes 3 and 4 are virtually identical (maximum difference of 0.9%), i.e. the solution on mesh 3 can be considered as good as grid independent. A similar conclusion can be drawn from Figure 5 (right), where the surface heat flux on meshes 3 and 4 overlap almost entirely in comparison with the coarser meshes (maximum difference of 2% at Z=0.03 [m]).

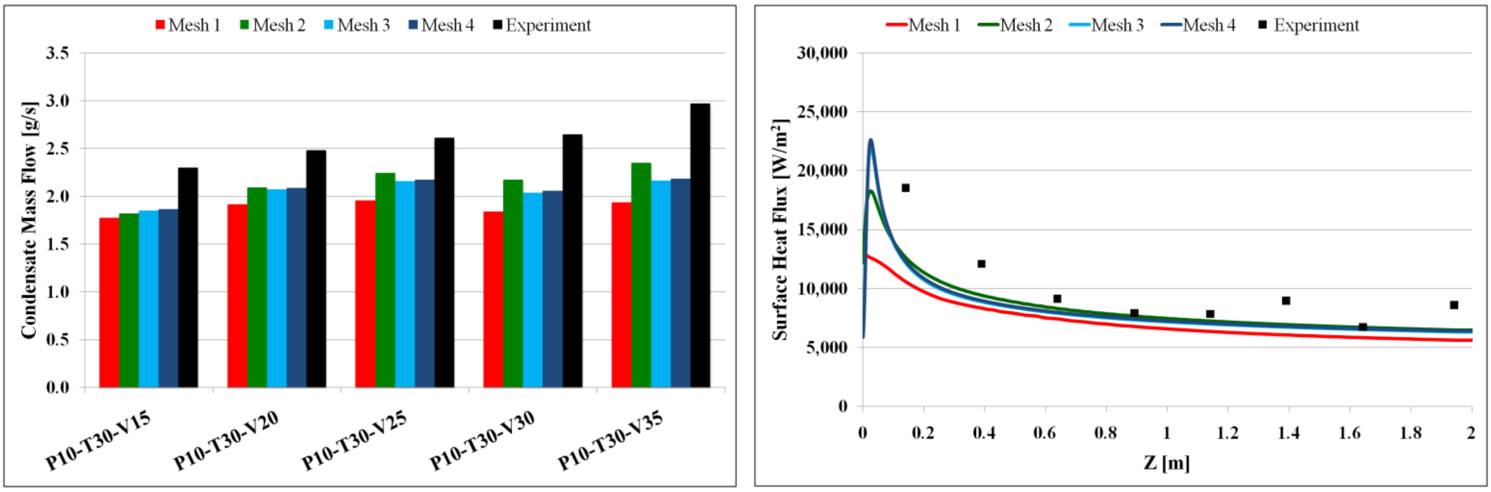

Figure 5. Condensation rate for different grid refinement levels (left). Surface heat flux as a function of Z for different meshes on experiment P10-T30-V25 (right)

Once the iteration and discretisation errors were quantified and reduced, the simulation results were compared against the experimental data as depicted in Figure 5. Although the CFD results match fairly well the experimental data trend, the present condensation model under-predicts both the surface heat flux and the condensation rate (average error of 20% w.r.t. experiments). This trend is similar to the CFD simulations reported by Ambrosini et al. (2008).

Since the turbulent quantities at the inlet of the primary test channel were not reported by Ambrosini et al. (2008), a sensitivity analysis was performed in ANSYS DesignXplorer 14.0. Figure 6 shows the response surface of the condensation rate obtained by varying the turbulence intensity and eddy viscosity ratio for experiment P10-T30-V25.

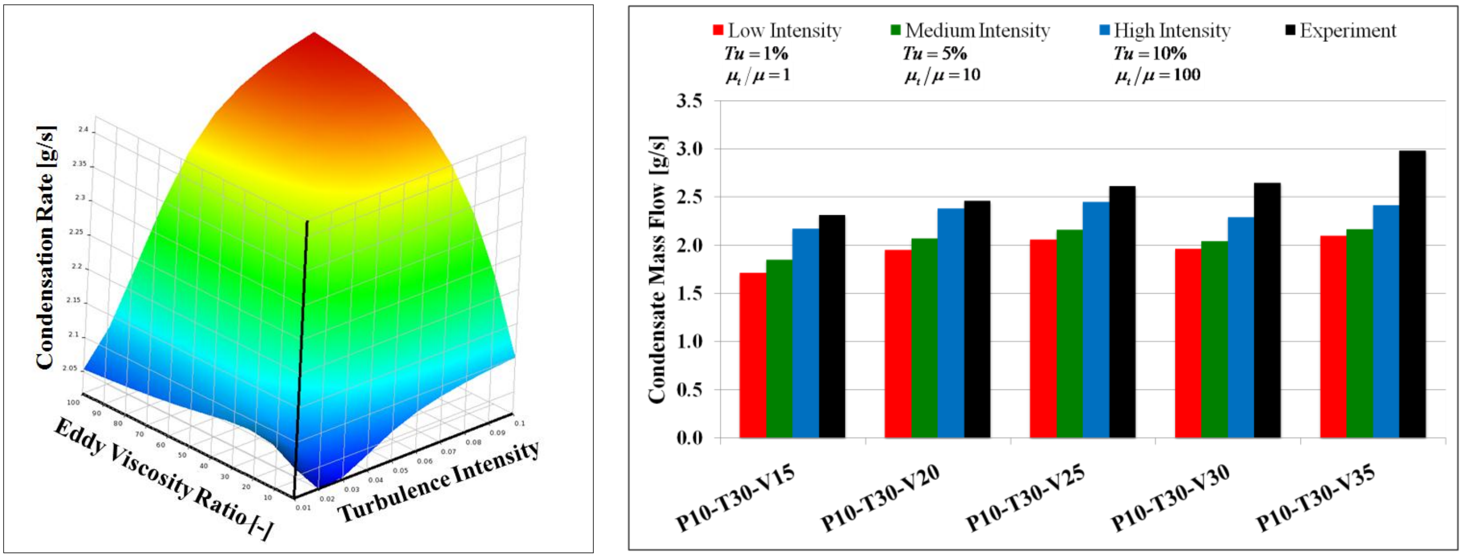

Figure 6. Surface response for the condensation rate as a function of the turbulence intensity and eddy viscosity ratio; experiment P10-T30-V25 (left). Condensation rate for different turbulence inlet boundary conditions (right)

The CFD calculations were carried out on several points laid out by a design of experiment method (central composite design). These results were fitted to a response surface by means of a second order polynomial. Here the condensation rate increases as both quantities increase, due to the enhanced turbulent transport of the water vapour towards the cooled plate.

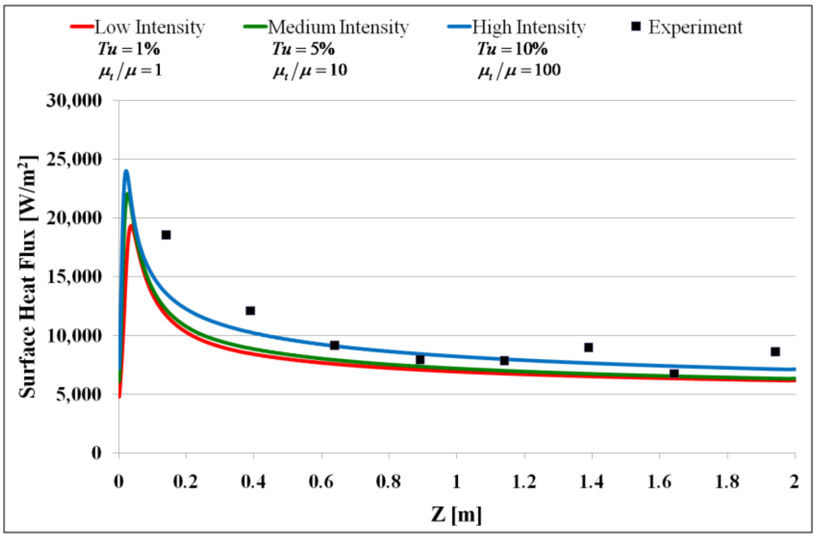

Figure 7. Surface heat flux for different turbulence inlet boundary conditions (exp. P10-T30-V25)

The general tendency observed in the response surface was further investigated for the condensation rate in all experimental points as shown in Figure 6 (right). Here the increase of the turbulent quantities leads to a better prediction of the condensation rate, especially for experiments P10-T30-V15 to P10-T30-V25. Similarly, the surface heat flux also increases as the turbulent quantities increases; leading to a better match with respect the experimental data (see Figure 7).

4. KUHN ET AL. TEST CASE

4.1. EXPERIMENTAL FACILITY

The second validation case is based on experiments by Kuhn et al. (1996, 1997). A schematic of the experimental test facility is shown in Figure 8. The test facility consists of a vertical inner condenser tube, where a mixture of steam and air is flowing downward. This steel condenser tube of 2 inches outer diameter and a wall thickness of 1.65mm is surrounded by an outer cylindrical water cooling jacket of 3 inches inner diameter which is designed to remove the heat from the steam-gas mixture and controls the steam wall condensation process. Cooling water is injected into this outer cooling jacket through two radial pipes at the bottom of the test facility and leaves through four radial pipes at the top. For the CFD simulations a 90° symmetry was assumed, i.e. the cooling water mass flow rate was distributed over 4 inlets at the bottom of the test facility, instead of the two inlet pipes in the real experiment.

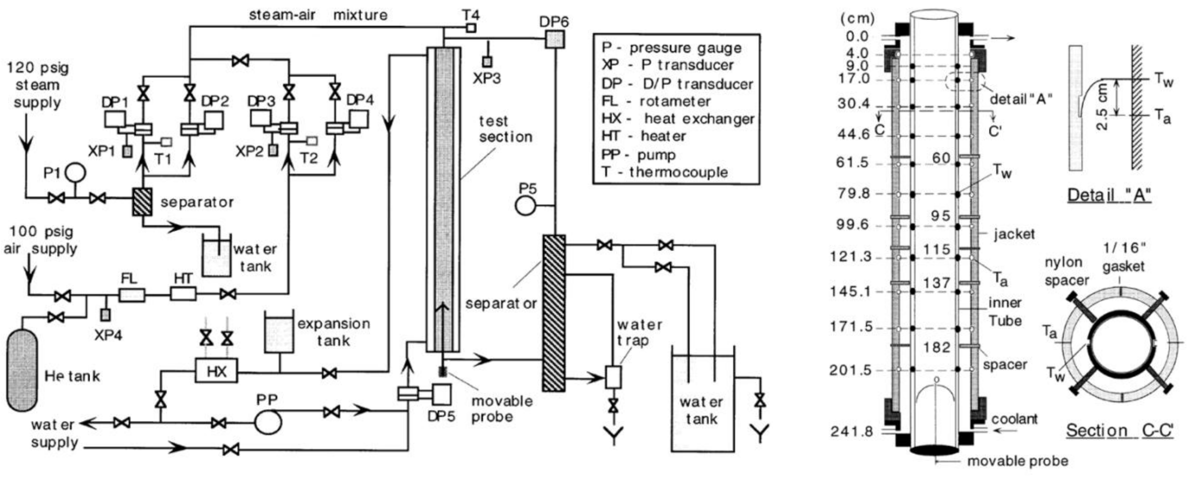

Figure 8. Schematic of the condenser tube and secondary cooling circuit of the test facility used by Kuhn et al. (1997)

Unfortunately Kuhn et al. have not applied any instrumentation which would have allowed measuring the steam condensation rate at the walls of the inner condenser tube. Instead the experiment by Kuhn et al. (1997) provides temperature measurements at the centreline (CL) of the condenser tube and at the inner wall (IW) of the cylindrical cooling water annulus over the height of the test facility. Since the latent heat of steam condensation massively influences the temperature of the gas mixture and wall temperatures, this is judged to provide an equally reliable measure for the accuracy of the applied phase change and wall condensation models. The selected test case conditions are summarized in Table 3.

Table 3. Conditions of the experiment 2.1-8R-Air by Kuhn et al. (1997)

Gas Mass Flow Rate [kg/h]	**Air Mass Fraction @ Inlet**	**Gas Inlet Temperature [°C]**	**Water Mass Flow Rate [kg/h]**	**Water Inlet Temperature [°C]**	**Pressure [kPa]**
Steam: 51.2 Air: 8.87	14.76%	145.5	925.1	27.5	413.1

4.2. GEOMETRY AND MESHING

Two series of CFD investigations have been carried out for the selected experimental conditions. First mesh independence of CFD results was investigated by applying the assumption, that the experimental test facility can be simplified to a two-dimensional geometry. Thereby it is assumed, that the flow in the outer cooling water jacket does not shown any pronounced three-dimensional inflow and outflow effects from the attached radial inlet and outlet pipes. In the second series of investigation, the geometry of the test facility was modelled in 3D assuming a 90° symmetry (see Figure 9). The three domains (fluid domain for the condenser tube, solid domain for the steel pipe and fluid domain for the water cooling jacket) of the test geometry have been constructed in the ANSYS DesignModeler 14.0.

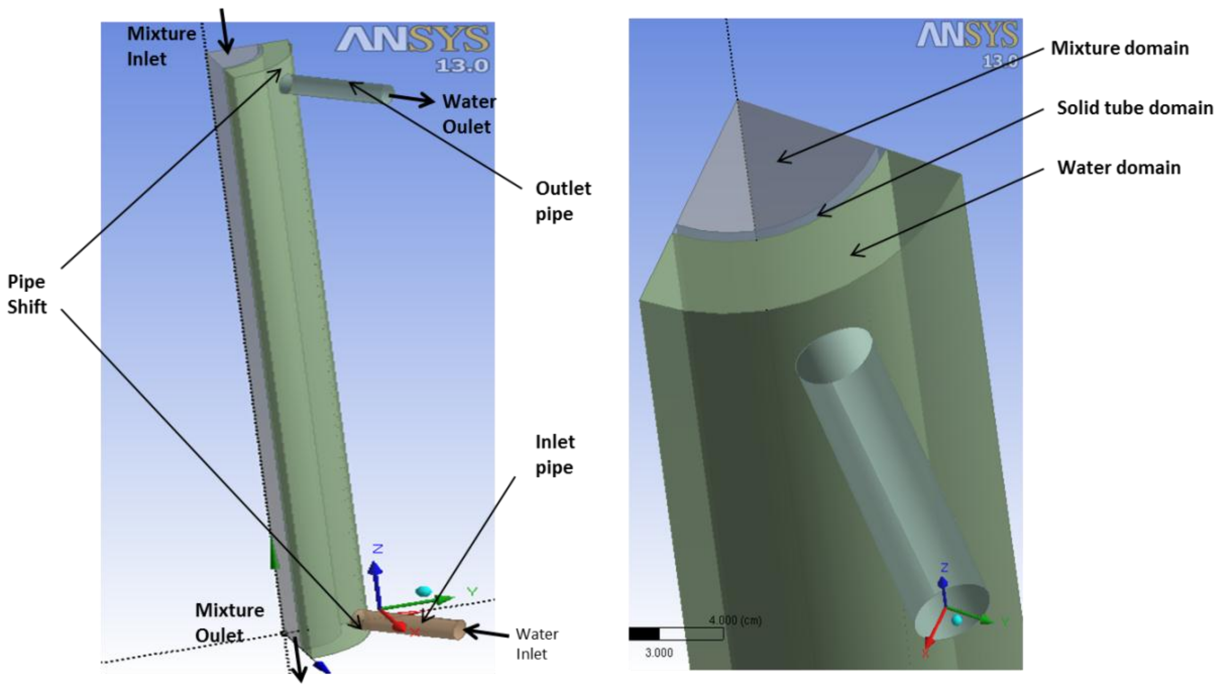

Figure 9. Three-dimensional geometry of the 90° symmetry sector for the CFD simulations

Hexahedral meshes were generated for all three domains in ANSYS ICEM CFD Hexa 14.0. Hierarchies of three 2D meshes and two 3D meshes have been created with a refinement factor of 2 in each coordinate direction. The properties of these grids are summarized in Table 4.

Table 4. 2D and 3D numerical grid properties

	2D Mesh 1	**2D Mesh 2**	**2D Mesh 3**	**3D Mesh 1**	**3D Mesh 2**
Number of Nodes	21,636	70,140	254,820	1,419,634	11,313,483
Number of Elements	13,172	44,336	165,080	1,500,340	11,637,400
Min. grid angle	45	45	45	24.1	21.1
Max. y^+ tube inner wall	8.3	4.8	3.1	4.6	1.9
Max. y^+ tube outer wall	3.4	1.6	0.8	3.7	1.1

4.3. CFD-SETUP AND BOUNDARY CONDITIONS

The steady-state simulations for the Kuhn et al. validation test case were performed using ANSYS CFX 14.0 using the coupled double precision solver. In the condenser tube the fluid was setup as an ideal multicomponent mixture of air and water steam, where air was treated as the constraint fluid material. The properties of air were modelled using the ideal gas equation of state and the water steam and condensate properties were modelled by means of the IAPWS-IF97 equation of state. For the IAPWS-IF97 tabulation a pressure range from 3[bar] to 5[bar] and the temperature range from 10[°C] to 200[°C] were applied. The IAPWS-IF97 tabulated properties were used for the cooling water as well. For the solid domain, the material properties of steel were taken from the ANSYS CFX standard material library.

The SST turbulence model by Menter (1994) was used for all calculations in conjunction with the automatic wall treatment for ω-based turbulence models. The wall condensation model was activated at the domain interface on the inner side of the condenser tube. Heat input into the steel wall of the condenser tube by turbulent convective heat flux from the air-steam mixture, by latent heat of condensation and by convective heat flux at the side of the cooling water annulus have been taken into account together with the conjugate heat transfer within the steel material of the tube.

The inlet boundary conditions for the inner condenser tube (air-steam mixture) and the cooling water flow in the outer annulus are summarized in Table 3. Since the turbulence boundary conditions were not specified by the experimentalists, a turbulence intensity of Tu=5% and an eddy viscosity ratio of $\mu_t/\mu=10$ were assumed at both inlets. For outlets of both systems an averaged static pressure boundary condition was applied. In addition a thermal boundary condition is required at the outer bounds of the CFD geometry. Since laboratory conditions were not specified in Kuhn et al. (1997) it was decided to use the third series of wall temperature measurements by Kuhn et al. at the outer wall of the cooling water annulus as a prescribed wall temperature boundary condition. A linear wall temperature profile from the bottom to the top of the outer cooling water jacket wall was used based on these data. For the bottom and top lid of the cooling water jacket as well as for the inlet and outlet cooling water pipes adiabatic wall boundary conditions had been assumed.

In the present case the solid and the air-water vapour mixture in the condenser tube were initialized with a temperature of 145.5[°C] and the water in the cooling jacket with a temperature of 27.5[°C]. It turned out that the latency of the conjugant heat transfer in the separating steel tube of the condenser was sufficient to lead to a moderate enough onset of the wall condensation process in the CFD simulations.

In the steady-state simulations a pseudo time-step of Δt =2[ms] was used for the fluid and solid domains. An under-relaxation factor of 0.1 was applied to the heat source of the wall condensation model. For the convergence criterion we used a maximum residual criterion of 10^{-4} and a conservation target of 0.001. For mass, momentum and energy conservation equations the second order upwind scheme (High Resolution) was applied and first order upwind scheme was used for the turbulence model equations. With those settings the CFD simulations reached the convergence target within approx. 850-900 iterations.

4.4. RESULTS

In a first series of two-dimensional CFD simulations the pseudo time-step and required depth of convergence were analysed. For the comparison of CFD results to data we use the fluid temperatures of the multicomponent mixture at the centreline of the condenser tube (CL) and the cooling water temperature over the height of the inner wall of the cooling water annulus (see Figure 8 for temperature sensor positions). The temperatures along the height of the outer wall of the cooling water annulus show a linear profile as prescribed at the thermal boundary condition. Figure 10 shows the comparison of the obtained fluid temperatures with data on the two-dimensional meshes of different spatial resolution. While the centreline temperature of the air-steam mixture is not sensitive to the mesh resolution, we observe mesh converged solution for the cooling water temperature at the surface of the condenser wall on mesh level 2, where results no longer change in comparison to mesh level 3. The obtained temperature profiles are in good agreement with the data reported by Kuhn et al. (1997) besides a small area at higher elevation, where three-dimensional effects of the cooling water outflow and the heat conduction in the top lid wall of the geometry seem to play an important role.

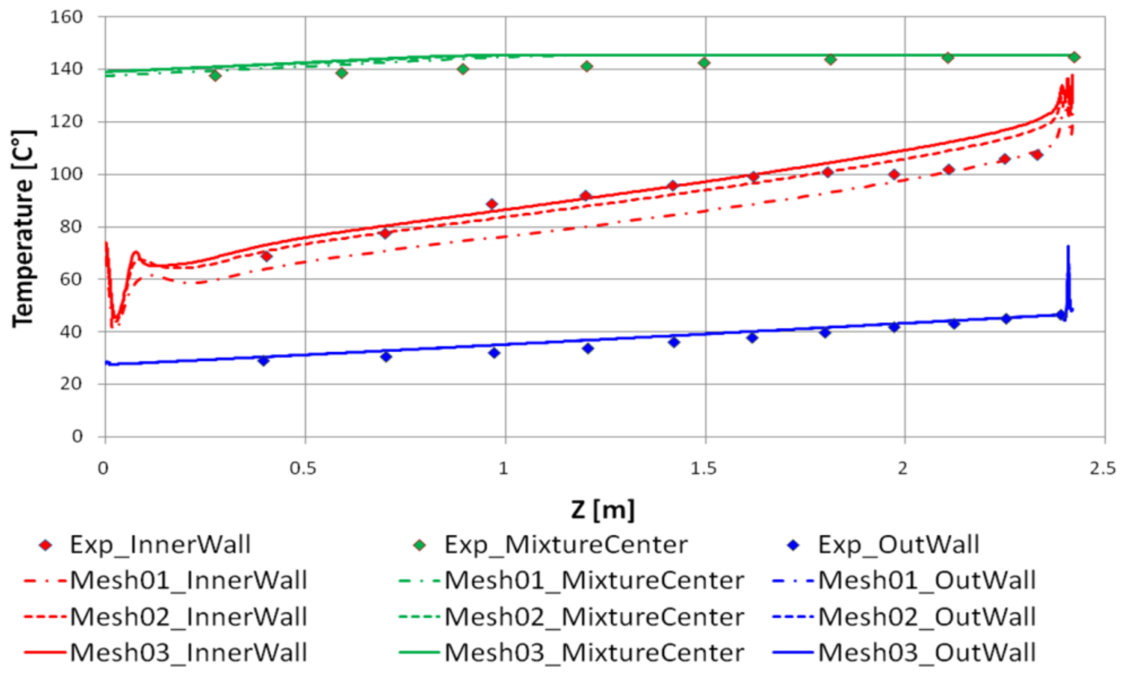

Figure 10. Mesh independence of predicted wall temperatures and comparison to data from the Run 2.1-8R experiment by Kuhn et al. (1997)

Further investigations have been carried out on the three-dimensional grids. Figure 11 shows the three-dimensional inlet and outlet flow effects in the cooling water jacket by representative streamlines. Figure 11 also shows the progressing steam condensation in the condenser tube during the downward flow of the air-steam mixture.

Comparing the predicted mixture temperature profile at the centerline of the condenser tube to data it can be observed from Figure 10 and Figure 12, that the mixture temperature at this location starts to drop slightly too late, i.e. at too low elevation in the condenser tube in comparison to experiment. But this measured temperature of the mixture is to a major extent a result of the turbulent mixing in the air-steam mixture in the condenser tube. Since turbulent inlet boundary conditions were not measured or specified, this is a major uncertainty in the present CFD simulations.

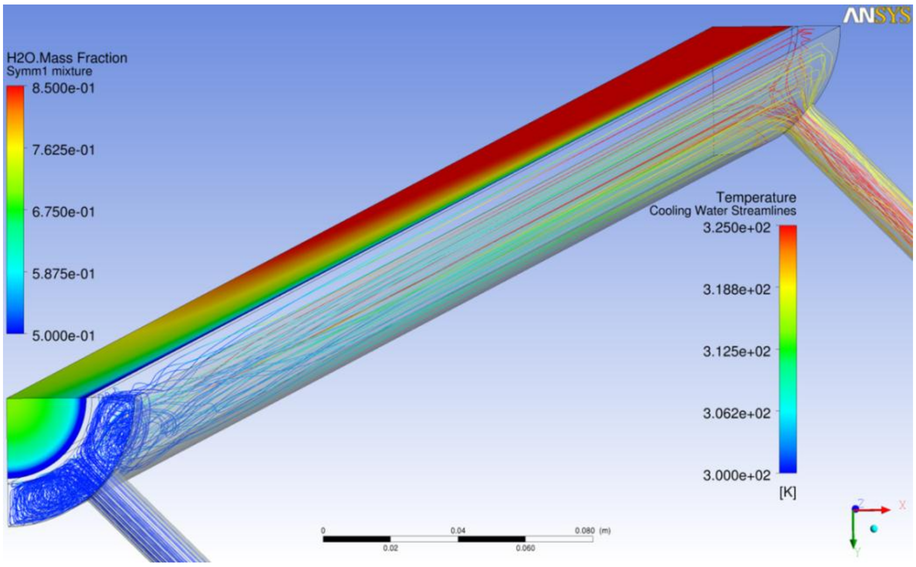

Figure 11. Water steam mass fraction and cooling water temperature along streamlines as predicted on the second 3D mesh

Finally Figure 12 shows the comparison of the experimental data with the two- and three-dimensional CFD results on the corresponding finest mesh levels. Here it can be seen, that the three-dimensional simulation leads to a substantially improved temperature wall profile at the inner wall of the water cooling jacket showing a logical drop of the water temperature to its inlet temperature at the lowest elevation. The deviation of the CFD results for the water temperatures at inner wall of the cooling water annulus at elevations z>1.8m could not be explained by the 3D simulations. Therefore it is assumed that the experimental test facility had some additional heat losses at the top lid of the water cooling jacket to the laboratory atmosphere (despite the specified insulation), which were not taken into account by the adiabatic wall boundary condition in the CFD simulations and which has finally led to the lower water temperatures in these locations.

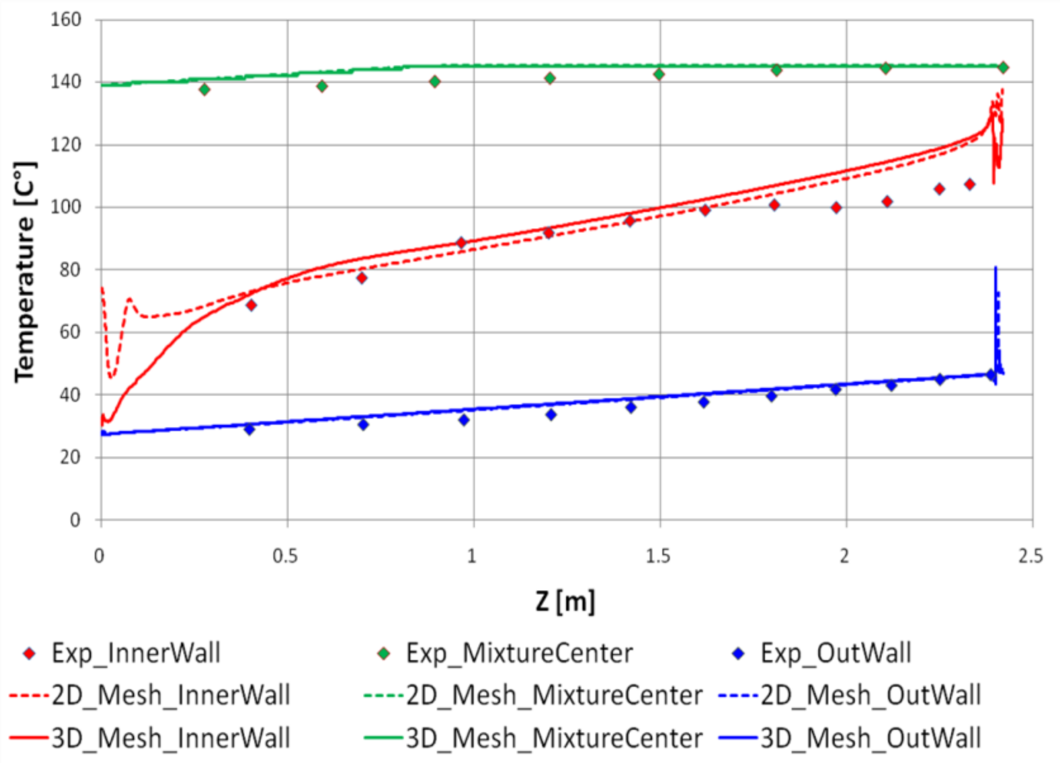

Figure 12. Comparison of temperature profiles on 2D Mesh 3 and 3D Mesh 2

5. SUMMARY AND CONCLUSION

The mathematical formulation of a newly implemented mathematical model for the simulation of wall condensation in the presence of non-condensable was presented along with its underlying assumptions. This mathematical model was validated with two laboratory scale experiments.

Iteration and discretisation errors were studied for the CONAN case. For the assumed turbulence boundary conditions at the inlet, the condensation rate and surface heat flux follow the trend of the experimental data, but the present model under-predicts their values. The sensitivity study shows that an increase of the turbulent intensity and eddy viscosity ratio increases both the condensation rate and surface heat flux, leading to a better agreement with the experimental data.

In the second validation case the spatial discretisation error was investigated as well as the effect of using 2D or 3D domains. The calculated centreline and inner wall temperature profiles are in good agreement with the experimental data reported by Kuhn et al. (1997). Three-dimensional effects at the inlet of the cooling water play an important role in the prediction of the water temperature profiles.

ACKNOWLEDGEMENTS

Supported by:
Federal Ministry of Economics and Technology
on the basis of a decision by the German Bundestag

The presented work is partially funded by the German Federal Ministry of Economics and Technology (BMWi, project number 1501415) on the basis of a decision by the German Bundestag.

REFERENCES

W.Ambrosini, N.Forgione, F.Oriolo, C.Dannöhl and H.J.Konle, “Experiments and CFD analyses on condensation heat transfer on a flat plate in a square cross section channel”, *Proc. 11th Int. Topical Meeting on Nuclear Reactor Thermal-Hydraulics, NURETH-11*, Avignon, France (2005).

W. Ambrosini, M. Bucci, N. Forgione, F. Oriolo, S. Paci, J.-P. Magnaud, E. Studer, E. Reinecke, St. Kelm, W. Jahn, J. Travis, H. Wilkening, M. Heitsch, I. Kljenak, M. Babić, M. Houkema, D.C. Visser, L. Vyskocil, P. Kostka and R. Huhtanen “Comparison and Analysis of the Condensation Benchmark Results”. *The 3rd European Review Meeting on Severe Accident Research (ERMSAR-2008)* Nessebar, Bulgaria, 23–25 September 2008.

R.B. Bird, W.E. Steward and E.N. Lightfoot. *Transport Phenomena*. John Wiley, New York, 1960.

J.C. de la Rosa, A. Escrivá, L.E. Herranz, T. Cicero and J.L. Muñoz-Cobo, “Review on condensation on the containment structures”, *Progress in Nuclear Energy*, 51, 32-66 (2009).

M. Houkema, N.B. Siccama, J.A. Lycklama à Nijeholt and E.M.J. Komen, “Validation of the CFX4 CFD code for containment thermal-hydraulics”, *Nuclear Engineering and Design*, 238, 590-599 (2008).

B.A. Kader, “Temperature and concentration profiles in fully turbulent boundary layers”, *International Journal of Heat and Mass Transfer*, 24(9), 1541-1544 (1981).

K. Karkoszka, H. Anglart, “Multidimensional effects in laminar filmwise condensation of water vapour in binary and ternary mixtures with noncondensable gases”, *Nuclear Engineering Design*, 238, 1373-1381 (2008)

S. Kelm, *Combination of a Building Condenser with H2-Recombiner Elements in Light Water Reactors,* Schriften des Forschungszentrums Jülich, 56 (2010).

S.Z. Kuhn, P.F. Peterson, V.E. Schrock, “Determination of the local heat flux in condensation experiments”, *Experimental Heat Transfer*, 9, 149-163 (1996).

S.Z. Kuhn, V.E. Schrock, P.F. Peterson, “An investigation of condensation from steam–gas mixtures flowing downward inside a vertical tube”, *Nuclear Engineering and Design*, 177, 53–69 (1997).

F. R. Menter.“Two-equation eddy-viscosity turbulence models for engineering applications”, *AIAA-Journal*, 32(8),1598-1605 (1994).

F. R. Menter. “CFD Best Practice Guidelines for CFD Code Validation for Reactor Safety Applications”, *Evaluation of Computational Fluid Dynamic Methods for Reactor Safety Analysis (ECORA),* European Commission, 5th EURATOM FRAMEWORK PROGRAMME, 1998-2002.

B.E. Poling, J.M. Prausnitz, J. O’Connell J. *The Properties of Gases and Liquids*. McGraw-Hill, New York, 2001.